Editors' Suggestion

Photonic Indistinguishability of the Tin-Vacancy Center in Nanostructured Diamond

Jesús Arjona Martínez,[1,*] Ryan A. Parker,[1,*] Kevin C. Chen,[2] Carola M. Purser,[1] Linsen Li,[2] Cathryn P. Michaels,[1] Alexander M. Stramma,[1] Romain Debroux,[1] Isaac B. Harris,[2] Martin Hayhurst Appel,[1] Eleanor C. Nichols,[1] Matthew E. Trusheim,[2] Dorian A. Gangloff,[1,3,†] Dirk Englund,[2,‡] and Mete Atatüre[1,§]

[1]*Cavendish Laboratory, University of Cambridge, JJ Thomson Avenue, Cambridge CB3 0HE, United Kingdom*

[2]*Department of Electrical Engineering and Computer Science, Massachusetts Institute of Technology, Cambridge, Massachusetts 02139, USA*

[3]*Department of Engineering Science, University of Oxford, Parks Road, Oxford OX1 3PJ, United Kingdom*

(Received 30 June 2022; accepted 28 September 2022; published 21 October 2022)

Tin-vacancy centers in diamond are promising spin-photon interfaces owing to their high quantum efficiency, large Debye-Waller factor, and compatibility with photonic nanostructuring. Benchmarking their single-photon indistinguishability is a key challenge for future applications. Here, we report the generation of single photons with $99.7^{+0.3}_{-2.5}\%$ purity and 63(9)% indistinguishability from a resonantly excited tin-vacancy center in a single-mode waveguide. We obtain quantum control of the optical transition with 1.71(1)-ns-long π pulses of 77.1(8)% fidelity and show it is spectrally stable over 100 ms. A modest Purcell enhancement factor of 12 would enhance the indistinguishability to 95%.

DOI: 10.1103/PhysRevLett.129.173603

Indistinguishable photons from quantum emitters provide a fundamental resource for scalable quantum communication and have been employed to realize linear optical quantum computation [1–3], spin-photon and spin-spin entanglement [4–6], and quantum repeater schemes [7–10]. Experimentally, the photonic indistinguishability can be benchmarked through two-photon quantum interference known as the Hong-Ou-Mandel (HOM) effect. The HOM indistinguishability places a bound on the fidelities achievable in photon-mediated gates and entanglement distribution in measurement-based protocols [11–13]. This effect has been observed across multiple solid-state emitters such as the nitrogen, silicon, and germanium vacancies in diamond [14–16], defects in silicon carbide [17], and semiconductor quantum dots [18].

Within solid-state emitters, the negatively charged group-IV centers in diamond stand as promising spin-photon interfaces due to their large Debye-Waller factor (60%–80%) [19–22], competitive quantum efficiency (10%–80%) [21–24], and first-order insensitivity to electric-field noise [25,26]. This electric-field agnosticism is compatible with complex photonic nanostructuring, as charge noise does not couple deleteriously to a proximate emitter. Accordingly, high collection efficiency [27,28], Purcell enhancement [29,30], and incorporation into photonic integrated circuits [31] have been demonstrated using group-IV centers embedded in diamond. The negatively charged tin-vacancy (SnV) is particularly promising. Its large ground-state orbital splitting inhibits phonon-mediated dephasing [32], allowing for operation at temperatures accessible in standard helium closed-cycle cryostats. Accordingly, it has shown a spin-coherence time (T_2) of 0.30(8) ms at 1.7 K [33], outperforming other group-IV centers at this temperature. Observation of transform-limited emission in nanopillars [34] and advancements in fabrication and charge stability [35] further demonstrate that SnV centers are a suitable spin-photon interface for quantum networking and measurement-based computation [12]. Confirming the optical coherence of the emitted photons is a necessary step toward these goals.

In this Letter, we report the observation of quantum interference of single photons from a SnV center in a single-mode diamond waveguide with an indistinguishability of 63(9)% and a single-photon purity of $99.7^{+0.3}_{-2.5}\%$. The orthogonal propagation directions of the excitation and collection modes, enabled by the waveguide nanostructure, suppress the excitation light by over 60 dB. We further realize coherent control of the optical transition of the SnV center with a π-rotation fidelity of 77.1(8)% performed in 1.71(1) ns. Thus, we show that the SnV center has sufficient photonic coherence to satisfy the requirements for quantum networking.

We perform our experiments on a diamond grown via chemical vapor deposition, implanted with Sn^{++} ions, annealed, and fabricated into a waveguide chiplet [36,37]. A chiplet consists of eight single-mode waveguides, each 50 μm long with a rectangular cross section of 200 nm by 270 nm. Figure 1(a) shows a characteristic device. The waveguides taper adiabatically over 9 μm at the ends to maximize the theoretical outcoupling efficiency [37]. A support diamond structure connects the waveguides, allowing the chiplet to be pick and placed onto a silicon substrate edge [31]. The SnV center fluorescence couples into a single-mode, lensed fiber giving a 23(3)-fold

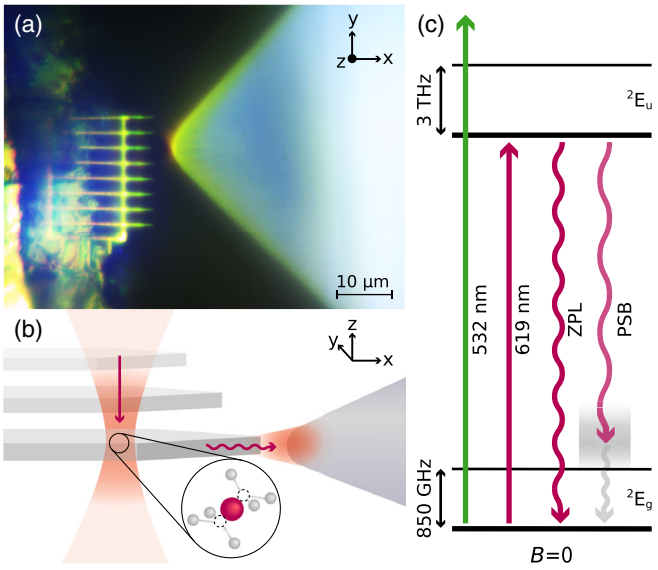

FIG. 1. (a) Microscope photograph of the lensed fiber aligned to a single waveguide using a three-axis nanopositioning stack. (b) Diagram of the excitation and collection geometry. (c) Electronic structure of the SnV center with no magnetic field. Off-resonant 532-nm and on-resonance 619-nm lasers generate emission into the ZPL and PSB radiative decay pathways.

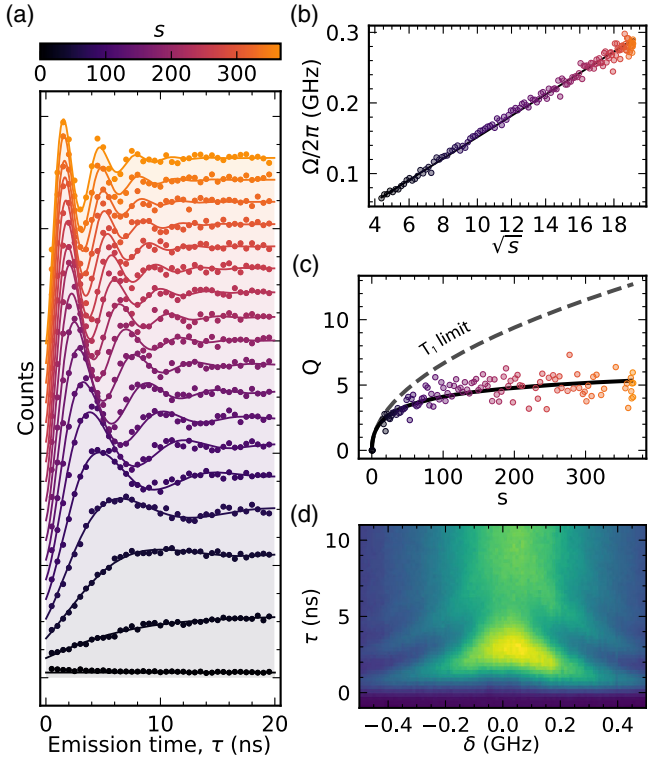

FIG. 2. (a) Histogrammed PSB fluorescence during a 20-ns-long resonant laser pulse. Curves are offset proportionally to the saturation parameter s. Solid curves are fits to a master equation [37]. At the highest saturation parameter, the excited-state population saturates to 0.5 at long times [37]. (b) Optical Rabi frequency Ω extracted from (a) as a function of $\sqrt{s}$. The black line is a linear fit with zero intercept. (c) Quality factor Q as a function of s. The solid black curve is a fit to a master equation including a pure dephasing rate proportional to Ω. The dashed black curve shows the absolute coherence limit. (d) Detuning δ dependence of the Rabi oscillations at $s = 102(4)$ for the same excitation scheme as (a). Color coding with blue (yellow) corresponds to low (high) fluorescence.

enhancement in collection efficiency relative to conventional confocal microscopy performed on the same emitter studied in this Letter [37].

Figure 1(b) shows the orthogonal excitation and collection directions. In this geometry, the continuous-wave laser suppression is over 60 dB. The fiber-coupled SnV fluorescence is then routed from inside the cryostat, held at 3.6 K, to our optical setup [37].

In the absence of a magnetic field, the SnV center has a spin-degenerate optical transition between the lower orbital branch of the ground state and the lower orbital branch of the excited state [52]. A 619-nm laser excites this transition resonantly, as highlighted in Fig. 1(c). Also highlighted are the two radiative-decay pathways, the zero-phonon line (ZPL) and phonon sideband (PSB). Resonant drive induces occasional blinking. To remedy this, we alternate between resonant and off-resonant 532-nm excitation [37], which pumps the emitter into the photoactive, -1 charge state [35]. The studied emitter has an excited-state lifetime T_1 of 7.44(20) ns, which corresponds to a transform-limited linewidth $\Gamma_0/2\pi$ of 21.4(2) MHz [37]. This is longer than the 5.0 ns reported for bulk diamond [22], likely due to the emitter being positioned close to the diamond-air interface [22,53].

We first demonstrate optical control of the SnV center through resonant excitation and collection of the PSB. Figure 2(a) shows the averaged PSB fluorescence during a 20-ns-long resonant 619-nm pulse starting at time $\tau = 0$. The histogrammed time-resolved fluorescence throughout the pulse is proportional to the instantaneous excited-state population and shows Rabi oscillations between the ground and excited states. The laser power P is parametrized by the saturation parameter $s = P/P_{\text{sat}}$, where $P_{\text{sat}} = 31(2)$ nW is the resonant laser power at which the Rabi rate Ω equals $\Gamma_0/\sqrt{2}$. For each power, the excited-state population is fit by a two-level master equation, to extract the corresponding Ω and dephasing rate [37,54,55]. An optical π rotation at the highest driving power [$s = 367(1)$] is performed in 1.71(1) ns, much faster than T_1, with a fidelity of 77.1(8)%.

To investigate the effects of decoherence, the master equation in Fig. 2(a) includes spontaneous emission and pure dephasing, as well as a shot-to-shot detuning fluctuation resulting in inhomogeneous dephasing [37]. We confirm in Fig. 2(b) a direct proportionality of the Rabi rate on the square root of the saturation parameter through the relationship $\Omega = \Gamma_0\sqrt{s/2}$. This linear relationship extends to our highest probed s and indicates that control-limiting

imperfections such as phonon coupling or multilevel driving do not cause an appreciable deviation from the master-equation model [37]. Figure 2(c) shows the power dependence of the quality factor Q, defined as the product of Ω and the $1/e$ envelope decay time extracted from the master-equation fits. In the low excitation power regime, Q increases with power and agrees with the limit set by T_1. At higher powers, Q saturates, which implies a laser-induced dephasing mechanism best modeled with a rate that linearly depends on Ω. Possible mechanisms could include photo-induced charge noise or resonant coupling to phononic modes [56–58].

By varying the frequency of the resonant laser, we also probe the dependence of the fluorescence on the detuning $\delta = \omega_l - \omega_0$, where ω_l and ω_0 are the angular frequencies of the 619-nm resonant laser and the transition, respectively. Figure 2(d) shows the time evolution of the fluorescence as a function of δ at $s = 102(4)$, yielding a Rabi rate of 153(3) MHz at $\delta = 0$ and faster, lower-amplitude, oscillations for $\delta \neq 0$. The ability to vary the detuning, phase, and amplitude of the resonant laser pulses enables multiaxis control of the optical qubit [37,56].

We next leverage multiaxis control to probe the coherence of the optical transition directly through pulsed resonant excitation. Figure 3(a) displays the measurements of Ramsey interferometry and Hahn-echo dynamical decoupling. We read out the state of the emitter by integrating the fluorescence after the final $\pi/2$ rotation. The population contrast between the ground and excited states is measured by varying the phase of this $\pi/2$ pulse [33,56]. The solid teal curve in Fig. 3(a) is a fit to the Ramsey-interferometry data using the master-equation model employed previously [37]. This yields an inhomogeneous dephasing time T_2^* of 4.54(2) ns, which corresponds to a shot-to-shot spectral drift of 82.6(5) MHz at full width at half maximum (FWHM). The Hahn-echo contrast decay envelope provides a measurement of the pure-dephasing rate Γ_{PD}. A fit to the raw contrast results in $\Gamma_{\mathrm{PD}}/2\pi = 6.39(14)$ MHz and an inferred homogeneous linewidth of $\Gamma/2\pi = (\Gamma_0 + 2\Gamma_{\mathrm{PD}})/2\pi = 34.8(7)$ MHz. This linewidth is only a factor of 1.63(4) from its intrinsic Fourier limit (Γ_0) despite the emitter's close proximity (< 60 nm) to nanostructured surfaces.

We next probe the spectral stability on longer timescales by observing the shot-to-shot variation of the transition frequency through fast photoluminescence excitation (PLE) scans at $s = 0.8(1)$. Each scan alternates between 500 ms of resonant 619-nm and off-resonant 532-nm excitation. During the resonant section, $\delta/2\pi$ is repeatedly scanned from -100 to 100 MHz using 3-μs-long linearly chirped laser pulses. Figure 3(b) shows the spectral evolution over 34 min. Within each vertical cut, and after correcting for power broadening, the linewidth is 35 (10) MHz, commensurate with the homogeneous linewidth inferred from the Hahn-echo measurement. This indicates

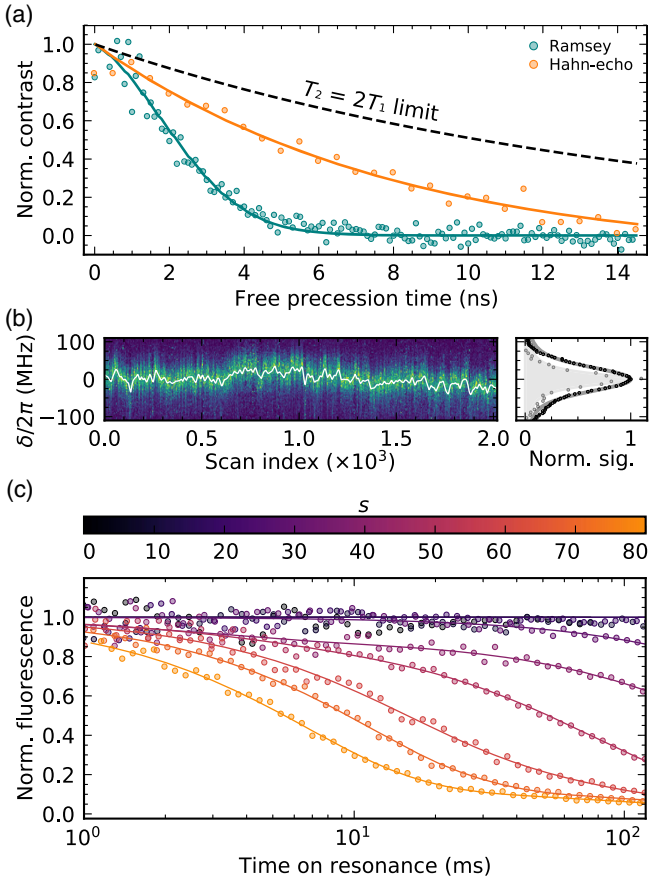

FIG. 3. (a) Measured Ramsey (teal) and Hahn-echo (orange) contrast decay envelopes with master-equation fits (solid curves) [37]. The dashed black curve is the absolute coherence limit, $T_2 = 2T_1$. The contrast at 0 ns is normalized to one. (b) Left: shot-to-shot evolution of the PLE line shape. Each vertical cut is the average of fast PLE scans over 500 ms. Off-resonant 532-nm excitation is applied between line cuts. The solid white line follows the emitter resonance frequency. Right: example line cut (gray) and inhomogeneous distribution of all line cuts (black), with Lorentzian and Gaussian fits, respectively. (c) Average PLE intensity as a function of time following a 532-nm off-resonant pulse for multiple saturation parameters. Solid curves are fits to biexponential decays. The experimental protocol is identical to that of (b). The dark-state pumping time is normalized by accounting for the fraction of time spent on resonance.

that there are no significant, additional, dephasing mechanisms present between the tens of nanoseconds timescale probed in Fig. 3(a) and the 500-ms timescale probed by the PLE scans in Fig. 3(b).

The central frequency does not show significant variation over consecutive scans. Over the entire measurement, it tends toward a normal distribution with a FWHM of 64(1) MHz. Such inhomogeneous broadening has been observed for the nitrogen-vacancy center [14], and, more recently, the SnV center [35], and is likely due to the off-resonant laser rearranging the local charge environment. For the nitrogen-vacancy center, the photoinduced spectral broadening

can be over 0.5 GHz or 35 times broader than the intrinsic linewidth [59]. In contrast, electric noise only detunes the SnV center through a second-order Stark shift [25], leading to a significantly narrower inhomogeneous linewidth. The deviation with respect to the Ramsey measurement could be attributed to the variation in 532-nm irradiation time. Figure 3(b) shows an inhomogeneous broadening of a factor of ∼2 compared to its homogeneous linewidth.

The 532-nm off-resonant excitation photostabilizes the emitter as resonant excitation pumps the emitter stochastically into a dark state [35]. To establish the timescale of this pumping, we monitor the decay of PLE intensity following a 532-nm off-resonant pulse. Repeatedly scanning 300 MHz across the transition ensures insensitivity to spectral diffusion. Figure 3(c) shows the decay of PSB fluorescence for various resonant excitation powers. The solid curves in Fig. 3(c) are fits to a biexponential model, where the dominant component is the fast timescale of pumping into the dark state. The slow timescale contributes 10(1)% of the total fluorescence at the highest power, likely due to a residual photoactive background [60,61]. The dark-state pumping rate increases linearly with s, in accordance with previous reports [35]. At the highest laser power, fluorescence persists over milliseconds, allowing $\sim 10^6$ π pulses to be applied before pumping into the dark state. When considered in concert with Fig. 3(b), our emitter remains spectrally stable and optically active over many milliseconds, as required for quantum networking [62].

To probe the indistinguishability of the emitted photons, we isolate the ZPL using spectral filtering. The residual resonant laser is suppressed by > 30 dB by pulsing the resonant excitation with two electro-optic modulators and time-tagging ZPL fluorescence after resonant excitation. Figure 4(a) shows the time-resolved ZPL fluorescence after a 4-ns resonant excitation pulse. The 90 dB total laser suppression yields a signal-to-background ratio of 23.91(3) for the ZPL fluorescence collected within 11.1 ns after the excitation pulse [37].

We measure a zero-delay second-order intensity correlation $g^{(2)}(0)_{\mathrm{raw}}$ of 0.067(23), as shown in Fig. 4(b) [63]. This is comparable to previous reports where only the PSB was collected, despite the added technical challenge of resonant collection in this Letter[33,34]. After correcting for detector dark counts, the background-corrected photon purity $[1 - g^{(2)}(0)]$ is $99.7^{+0.3}_{-2.5}\%$.

Figure 4(c) shows our HOM-interferometry setup [37]. Before the interferometer, a dichroic mirror and a grating filter photons within a 245(6) GHz bandwidth (FWHM)

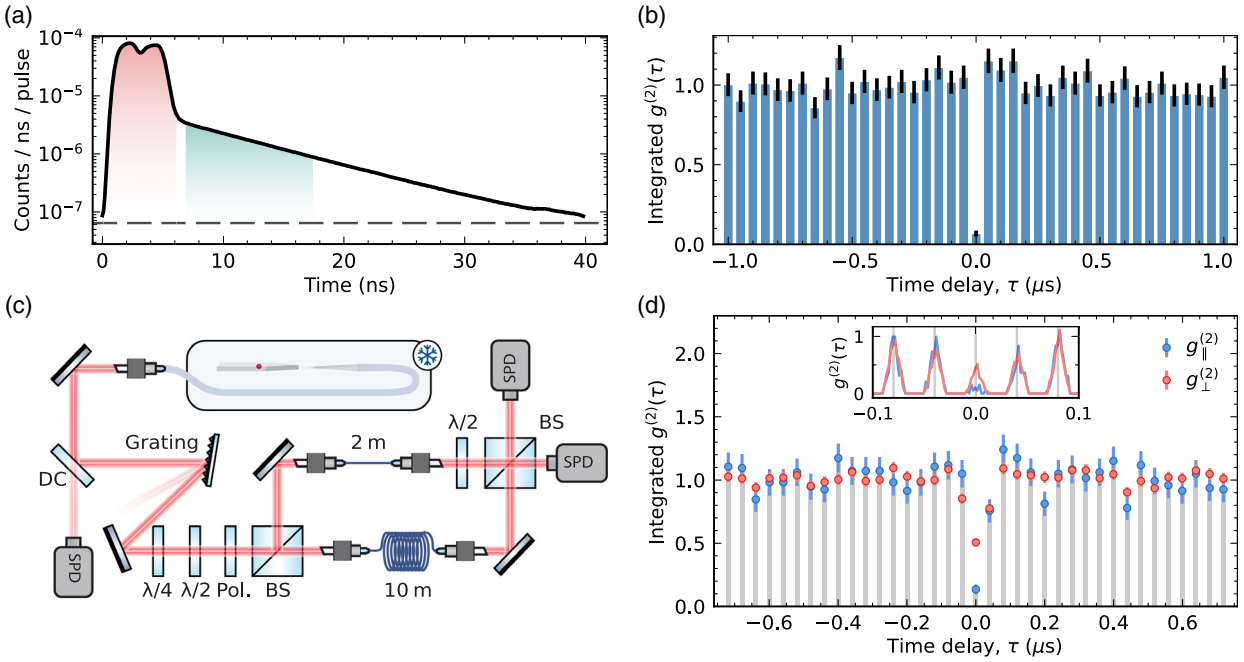

FIG. 4. (a) Time-resolved ZPL fluorescence under excitation with a 4-ns-long resonant laser pulse, at $s = 45(20)$. Red and teal shadings correspond to applied laser excitation and ZPL fluorescence collection, respectively. The average background (dashed line) is extracted with a far-detuned ($\delta/2\pi = 6$ GHz) laser pulse [37]. (b) Second-order autocorrelation of the ZPL fluorescence under pulsed resonant excitation. The recorded value $g^{(2)}(0)_{\mathrm{raw}} = 0.067(23)$ corresponds to a background-corrected photon purity of $99.7^{+0.3}_{-2.5}\%$. (c) Experimental setup for the HOM measurement. Abbreviations: quarter-wave plate ($\lambda/4$), half-wave plate ($\lambda/2$), polarizer (Pol.), beam splitter (BS), and dichroic mirror (DC). (d) Pulsed two-photon interference measurement for the parallel (blue) and perpendicular (red) polarization configurations, where the coincidence counts are integrated for each pulse. The background-corrected photon indistinguishability is 73(13)% for photons collected within the teal region in (a). Inset: time-resolved distribution of coincidences around $\tau = 0$.

centered on the ZPL transition. This filtered emission is routed through polarization control optics and into the interferometer with a relative time delay Δt of 39.93(2) ns between the two arms. To ensure temporal overlap between subsequently emitted photons, we apply laser pulses with a repetition period matching Δt. A half-wave plate placed in the short arm of the interferometer controls the relative polarization between the two interfering photons.

Figure 4(d) shows the second-order intensity correlation measured across the two output ports of the interferometer for ZPL fluorescence integrated over the first 11.1 ns after the excitation pulse. When the polarizations of two interfering photons are orthogonal to each other, we measure $g_{\perp}^{(2)}(0) = 0.51(3)$, in agreement with the theoretically expected value of 0.5. When the polarizations of the photons are matched, we measure $g_{\parallel}^{(2)}(0) = 0.22(3)$. The raw visibility $V_{\mathrm{raw}} = 1 - g_{\parallel}^{(2)}(0)/g_{\perp}^{(2)}(0) = 56(8)\%$ is a measurement of the indistinguishability of the emitted photons. Correcting for the background and finite classical interferometric contrast, we calculate a photon indistinguishability V of 73(13)%. When the time window is extended to the full decay observed in Fig. 4(a), the indistinguishability is reduced to $V = 63(9)\%$ [37].

We compare our measured indistinguishability to a model that includes homogeneous broadening as the source of photon distinguishability. Given the measured Γ_{PD}, the expected HOM visibility V_{sim} is 63.2(4)%, in agreement with our measured value [37]. Considering the slow spectral diffusion measured in Fig. 3(b), the HOM visibility measured here should extend to interferometer delays greater than 100 ms.

In this Letter, we demonstrate coherent control of the optical transition of the SnV in diamond. We achieve a π-pulse time of 1.71(1) ns and two-photon quantum interference of resonant photons with an indistinguishability of 63(9)%. Purcell enhancement of the emitter, such as through optical microcavities [64] or photonic crystal cavities [28–30], increases the radiative decay rate and, thus, reduces the sensitivity to dephasing. An overall Purcell enhancement factor of 12, already achieved using SnV centers in nanocavities [29,30], would yield a photon indistinguishability in excess of 95%. Moreover, fabrication and material processing improvements, known to result in improved optical quality of SnV centers in bulk diamond [22], should enhance the optical coherence. These advancements provide a feasible route to near-unity photon indistinguishability in the near term.

Using the two-photon interference presented in this Letter, in combination with control of the spin degree of freedom [33], one could realize spin-photon entanglement [5,65,66] and entanglement of remote emitters [4,67,68]. Modest improvements in the indistinguishability of the photons would position multiphoton entangled states as the next achievement using the SnV center [69,70].

The data that support the findings of this study are available upon reasonable request from the corresponding authors.

We acknowledge support from the ERC Advanced Grant PEDESTAL (884745), the EU Quantum Flagship 2D-SIPC. J. A. M. acknowledges support from the Winton Program and EPSRC DTP; R. A. P. from the General Sir John Monash Foundation; K. C. C. from the National Science Foundation Graduate Research Fellowships Program (GRFP) and the NSF STC Center for Integrated Quantum Materials (CIQM), NSF Grant No. DMR-1231319, and NSF Grant No. 1839155; C. P. M. from the EPSRC DTP; A. M. S. from EPSRC/NQIT; R. D. from the Gates Cambridge Trust; M. E. T. from the Army Research Laboratory ENIAC Distinguished Postdoctoral Fellowship; and D. A. G. from a St. John's College Title A Fellowship and a Royal Society University Research Fellowship. D. E. acknowledges further support by the MITRE Quantum Moonshot Program.

*These authors contributed equally to this work.
†Corresponding author.
dorian.gangloff@eng.ox.ac.uk
‡Corresponding author.
englund@mit.edu
§Corresponding author.
ma424@cam.ac.uk

[1] S. D. Barrett and P. Kok, Efficient high-fidelity quantum computation using matter qubits and linear optics, Phys. Rev. A **71**, 060310(R) (2005).
[2] B. P. Lanyon, P. Jurcevic, M. Zwerger, C. Hempel, E. A. Martinez, W. Dür, H. J. Briegel, R. Blatt, and C. F. Roos, Measurement-Based Quantum Computation with Trapped Ions, Phys. Rev. Lett. **111**, 210501 (2013).
[3] H. Wang, J. Qin, X. Ding, M.-C. Chen, S. Chen, X. You, Y.-M. He, X. Jiang, L. You, Z. Wang *et al.*, Boson Sampling with 20 Input Photons and a 60-Mode Interferometer in a 1 0 14-Dimensional Hilbert Space, Phys. Rev. Lett. **123**, 250503 (2019).
[4] C. Cabrillo, J. I. Cirac, P. Garcia-Fernandez, and P. Zoller, Creation of entangled states of distant atoms by interference, Phys. Rev. A **59**, 1025 (1999).
[5] R. Vasconcelos, S. Reisenbauer, C. Salter, G. Wachter, D. Wirtitsch, J. Schmiedmayer, P. Walther, and M. Trupke, Scalable spin–photon entanglement by time-to-polarization conversion, npj Quantum Inf. **6**, 9 (2020).
[6] H. Bernien, B. Hensen, W. Pfaff, G. Koolstra, M. S. Blok, L. Robledo, T. H. Taminiau, M. Markham, D. J. Twitchen, L. Childress, and R. Hanson, Heralded entanglement between solid-state qubits separated by three metres, Nature (London) **497**, 86 (2013).
[7] Z.-S. Yuan, Y.-A. Chen, B. Zhao, S. Chen, J. Schmiedmayer, and J.-W. Pan, Experimental demonstration of a BDCZ quantum repeater node, Nature (London) **454**, 1098 (2008).

[8] K. Azuma, K. Tamaki, and H.-K. Lo, All-photonic quantum repeaters, Nat. Commun. **6**, 1 (2015).
[9] Z.-D. Li, R. Zhang, X.-F. Yin, L.-Z. Liu, Y. Hu, Y.-Q. Fang, Y.-Y. Fei, X. Jiang, J. Zhang, L. Li *et al.*, Experimental quantum repeater without quantum memory, Nat. Photonics **13**, 644 (2019).
[10] D. Lago-Rivera, S. Grandi, J. V. Rakonjac, A. Seri, and H. de Riedmatten, Telecom-heralded entanglement between multimode solid-state quantum memories, Nature (London) **594**, 37 (2021).
[11] C.-K. Hong, Z.-Y. Ou, and L. Mandel, Measurement of Subpicosecond Time Intervals between Two Photons by Interference, Phys. Rev. Lett. **59**, 2044 (1987).
[12] M. Zwerger, H. Briegel, and W. Dür, Measurement-based quantum communication, Appl. Phys. B **122**, 50 (2016).
[13] T. Rudolph, Why I am optimistic about the silicon-photonic route to quantum computing, APL Photonics **2**, 030901 (2017).
[14] H. Bernien, L. Childress, L. Robledo, M. Markham, D. Twitchen, and R. Hanson, Two-Photon Quantum Interference from Separate Nitrogen Vacancy Centers in Diamond, Phys. Rev. Lett. **108**, 043604 (2012).
[15] A. Sipahigil, K. D. Jahnke, L. J. Rogers, T. Teraji, J. Isoya, A. S. Zibrov, F. Jelezko, and M. D. Lukin, Indistinguishable Photons from Separated Silicon-Vacancy Centers in Diamond, Phys. Rev. Lett. **113**, 113602 (2014).
[16] D. Chen, J. E. Frch, S. Ru, H. Cai, N. Wang, G. Adamo, J. Scott, F. Li, N. Zheludev, I. Aharonovich, and W. Gao, Quantum interference of resonance fluorescence from germanium-vacancy color centers in diamond, Nano Lett. **22**, 6306 (2022).
[17] N. Morioka, C. Babin, R. Nagy, I. Gediz, E. Hesselmeier, D. Liu, M. Joliffe, M. Niethammer, D. Dasari, V. Vorobyov *et al.*, Spin-controlled generation of indistinguishable and distinguishable photons from silicon vacancy centres in silicon carbide, Nat. Commun. **11**, 2516 (2020).
[18] C. Santori, D. Fattal, J. Vučković, G. S. Solomon, and Y. Yamamoto, Indistinguishable photons from a single-photon device, Nature (London) **419**, 594 (2002).
[19] E. Neu, M. Fischer, S. Gsell, M. Schreck, and C. Becher, Fluorescence and polarization spectroscopy of single silicon vacancy centers in heteroepitaxial nanodiamonds on iridium, Phys. Rev. B **84**, 205211 (2011).
[20] Y. N. Palyanov, I. N. Kupriyanov, Y. M. Borzdov, and N. V. Surovtsev, Germanium: A new catalyst for diamond synthesis and a new optically active impurity in diamond, Sci. Rep. **5**, 14789 (2015).
[21] M. K. Bhaskar, D. D. Sukachev, A. Sipahigil, R. E. Evans, M. J. Burek, C. T. Nguyen, L. J. Rogers, P. Siyushev, M. H. Metsch, H. Park *et al.*, Quantum Nonlinear Optics with a Germanium-Vacancy Color Center in a Nanoscale Diamond Waveguide, Phys. Rev. Lett. **118**, 223603 (2017).
[22] J. Görlitz, D. Herrmann, G. Thiering, P. Fuchs, M. Gandil, T. Iwasaki, T. Taniguchi, M. Kieschnick, J. Meijer, M. Hatano *et al.*, Spectroscopic investigations of negatively charged tin-vacancy centres in diamond, New J. Phys. **22**, 013048 (2020).
[23] D. D. Sukachev, A. Sipahigil, C. T. Nguyen, M. K. Bhaskar, R. E. Evans, F. Jelezko, and M. D. Lukin, Silicon-Vacancy Spin Qubit in Diamond: A Quantum Memory Exceeding 10 ms with Single-Shot State Readout, Phys. Rev. Lett. **119**, 223602 (2017).
[24] T. Iwasaki, Y. Miyamoto, T. Taniguchi, P. Siyushev, M. H. Metsch, F. Jelezko, and M. Hatano, Tin-Vacancy Quantum Emitters in Diamond, Phys. Rev. Lett. **119**, 253601 (2017).
[25] L. De Santis, M. E. Trusheim, K. C. Chen, and D. R. Englund, Investigation of the Stark Effect on a Centrosymmetric Quantum Emitter in Diamond, Phys. Rev. Lett. **127**, 147402 (2021).
[26] G. Thiering and A. Gali, Ab Initio Magneto-Optical Spectrum of Group-IV Vacancy Color Centers in Diamond, Phys. Rev. X **8**, 021063 (2018).
[27] E. N. Knall, C. M. Knaut, R. Bekenstein, D. R. Assumpcao, P. L. Stroganov, W. Gong, Y. Q. Huan, P.-J. Stas, B. Machielse, M. Chalupnik *et al.*, Efficient Source of Shaped Single Photons Based on an Integrated Diamond Nanophotonic System, Phys. Rev. Lett. **129**, 053603 (2022).
[28] M. K. Bhaskar, R. Riedinger, B. Machielse, D. S. Levonian, C. T. Nguyen, E. N. Knall, H. Park, D. Englund, M. Lončar, D. D. Sukachev, and M. D. Lukin, Experimental demonstration of memory-enhanced quantum communication, Nature (London) **580**, 60 (2020).
[29] A. E. Rugar, S. Aghaeimeibodi, D. Riedel, C. Dory, H. Lu, P. J. McQuade, Z.-X. Shen, N. A. Melosh, and J. Vučković, Quantum Photonic Interface for Tin-Vacancy Centers in Diamond, Phys. Rev. X **11**, 031021 (2021).
[30] K. Kuruma, B. Pingault, C. Chia, D. Renaud, P. Hoffmann, S. Iwamoto, C. Ronning, and M. Lončar, Coupling of a single tin-vacancy center to a photonic crystal cavity in diamond, Appl. Phys. Lett. **118**, 230601 (2021).
[31] N. H. Wan, T.-J. Lu, K. C. Chen, M. P. Walsh, M. E. Trusheim, L. De Santis, E. A. Bersin, I. B. Harris, S. L. Mouradian, I. R. Christen *et al.*, Large-scale integration of artificial atoms in hybrid photonic circuits, Nature (London) **583**, 226 (2020).
[32] C. Bradac, W. Gao, J. Forneris, M. E. Trusheim, and I. Aharonovich, Quantum nanophotonics with group IV defects in diamond, Nat. Commun. **10**, 5625 (2019).
[33] R. Debroux, C. P. Michaels, C. M. Purser, N. Wan, M. E. Trusheim, J. Arjona Martínez, R. A. Parker, A. M. Stramma, K. C. Chen, L. de Santis, Evgeny M. Alexeev, Andrea C. Ferrari, Dirk Englund, Dorian A. Gangloff, and Mete Atatüre, Quantum Control of the Tin-Vacancy Spin Qubit in Diamond, Phys. Rev. X **11**, 041041 (2021).
[34] M. E. Trusheim, B. Pingault, N. H. Wan, M. Gündoğan, L. De Santis, R. Debroux, D. Gangloff, C. Purser, K. C. Chen, M. Walsh *et al.*, Transform-Limited Photons from a Coherent Tin-Vacancy Spin in Diamond, Phys. Rev. Lett. **124**, 023602 (2020).
[35] J. Görlitz, D. Herrmann, P. Fuchs, T. Iwasaki, T. Taniguchi, D. Rogalla, D. Hardeman, P.-O. Colard, M. Markham, M. Hatano, and C. Becher, Coherence of a charge stabilised tin-vacancy spin in diamond, npj Quantum Inf. **8**, 45 (2022).
[36] S. Mouradian, N. H. Wan, T. Schröder, and D. Englund, Rectangular photonic crystal nanobeam cavities in bulk diamond, Appl. Phys. Lett. **111**, 021103 (2017).
[37] See Supplemental Material at http://link.aps.org/supplemental/10.1103/PhysRevLett.129.173603 for information on experimental methods, theoretical simulations, and extended data analysis, which includes Refs. [38–51].

[38] J. F. Ziegler and J. P. Biersack, The stopping and range of ions in matter, in *Treatise on Heavy-Ion Science* (Springer, New York, 1985), pp. 93–129.
[39] N. H. Wan, S. Mouradian, and D. Englund, Two-dimensional photonic crystal slab nanocavities on bulk single-crystal diamond, Appl. Phys. Lett. **112**, 141102 (2018).
[40] S. Sangtawesin, B. L. Dwyer, S. Srinivasan, J. J. Allred, L. V. H. Rodgers, K. De Greve, A. Stacey, N. Dontschuk, K. M. O'Donnell, D. Hu, D. A. Evans, C. Jaye, D. A. Fischer, M. L. Markham, D. J. Twitchen, H. Park, M. D. Lukin, and N. P. de Leon, Origins of Diamond Surface Noise Probed by Correlating Single-Spin Measurements with Surface Spectroscopy, Phys. Rev. X **9**, 031052 (2019).
[41] S. L. Mouradian, T. Schröder, C. B. Poitras, L. Li, J. Goldstein, E. H. Chen, M. Walsh, J. Cardenas, M. L. Markham, D. J. Twitchen *et al.*, Scalable Integration of Long-Lived Quantum Memories into a Photonic Circuit, Phys. Rev. X **5**, 031009 (2015).
[42] F. A. Inam, A. M. Edmonds, M. J. Steel, and S. Castelletto, Tracking emission rate dynamics of nitrogen vacancy centers in nanodiamonds, Appl. Phys. Lett. **102**, 253109 (2013).
[43] G. Lindblad, On the generators of quantum dynamical semigroups, Commun. Math. Phys. **48**, 119 (1976).
[44] J. F. Barry, J. M. Schloss, E. Bauch, M. J. Turner, C. A. Hart, L. M. Pham, and R. L. Walsworth, Sensitivity optimization for nv-diamond magnetometry, Rev. Mod. Phys. **92**, 015004 (2020).
[45] M. H. Appel, A quantum dot source of time-bin multi-photon entanglement, Ph.D. thesis, Niels Bohr Institute, 2021.
[46] A. Bechtold, D. Rauch, F. Li, T. Simmet, P.-L. Ardelt, A. Regler, K. Müller, N. A. Sinitsyn, and J. J. Finley, Three-stage decoherence dynamics of an electron spin qubit in an optically active quantum dot, Nat. Phys. **11**, 1005 (2015).
[47] G. Éthier-Majcher, D. Gangloff, R. Stockill, E. Clarke, M. Hugues, C. Le Gall, and M. Atatüre, Improving a Solid-State Qubit through an Engineered Mesoscopic Environment, Phys. Rev. Lett. **119**, 130503 (2017).
[48] R. Stockill, C. Le Gall, C. Matthiesen, L. Huthmacher, E. Clarke, M. Hugues, and M. Atatüre, Quantum dot spin coherence governed by a strained nuclear environment, Nat. Commun. **7**, 12745 (2016).
[49] B. Kambs and C. Becher, Limitations on the indistinguishability of photons from remote solid state sources, New J. Phys. **20**, 115003 (2018).
[50] A. M. Brańczyk, Hong-ou-mandel interference, arXiv: 1711.00080.
[51] N. Tomm, A quantum dot in a microcavity as a bright source of coherent single photons, Ph.D. thesis, University of Basel, 2021.
[52] C. Hepp, T. Müller, V. Waselowski, J. N. Becker, B. Pingault, H. Sternschulte, D. Steinmüller-Nethl, A. Gali, J. R. Maze, M. Atatüre, and C. Becher, Electronic Structure of the Silicon Vacancy Color Center in Diamond, Phys. Rev. Lett. **112**, 036405 (2014).
[53] D. Jalas, K. M. Schulz, A. Y. Petrov, and M. Eich, Emission enhancement in dielectric nanocomposites, Opt. Express **26**, 16352 (2018).
[54] V. Gorini, A. Kossakowski, and E. C. G. Sudarshan, Completely positive dynamical semigroups of N-level systems, J. Math. Phys. (N.Y.) **17**, 821 (1976).
[55] G. Lindblad, On the generators of quantum dynamical semigroups, Commun. Math. Phys. **48**, 119 (1976).
[56] J. Bodey, R. Stockill, E. Denning, D. Gangloff, G. Éthier-Majcher, D. Jackson, E. Clarke, M. Hugues, C. L. Gall, and M. Atatüre, Optical spin locking of a solid-state qubit, npj Quantum Inf. **5**, 95 (2019).
[57] A. J. Ramsay, A. V. Gopal, E. M. Gauger, A. Nazir, B. W. Lovett, A. M. Fox, and M. S. Skolnick, Damping of Exciton Rabi Rotations by Acoustic Phonons in Optically Excited InGaAs/GaAs Quantum Dots, Phys. Rev. Lett. **104**, 017402 (2010).
[58] J. Iles-Smith, D. P. McCutcheon, A. Nazir, and J. Mørk, Phonon limit to simultaneous near-unity efficiency and indistinguishability in semiconductor single photon sources, in *CLEO: QELS Fundamental Science* (Optical Society of America, Washington, DC, 2017).
[59] P. Siyushev, H. Pinto, M. Vörös, A. Gali, F. Jelezko, and J. Wrachtrup, Optically Controlled Switching of the Charge State of a Single Nitrogen-Vacancy Center in Diamond at Cryogenic Temperatures, Phys. Rev. Lett. **110**, 167402 (2013).
[60] R. Parker, N. Dontschuk, S.-I. Sato, C.-K. Lew, P. Reineck, A. Nadarajah, T. Ohshima, B. Gibson, S. Castelletto, J. McCallum, and B. C. Johnson, Infrared erbium photoluminescence enhancement in silicon carbide nano-pillars, J. Appl. Phys. **130**, 145101 (2021).
[61] J. T. Choy, B. J. Hausmann, T. M. Babinec, I. Bulu, M. Khan, P. Maletinsky, A. Yacoby, and M. Lončar, Enhanced single-photon emission from a diamond–silver aperture, Nat. Photonics **5**, 738 (2011).
[62] M. Pompili, S. L. Hermans, S. Baier, H. K. Beukers, P. C. Humphreys, R. N. Schouten, R. F. Vermeulen, M. J. Tiggelman, L. dos Santos Martins, B. Dirkse *et al.*, Realization of a multinode quantum network of remote solid-state qubits, Science **372**, 259 (2021).
[63] R. Brown and R. Q. Twiss, Correlation between photons in two coherent beams of light, Nature (London) **177**, 27 (1956).
[64] D. Riedel, I. Söllner, B. J. Shields, S. Starosielec, P. Appel, E. Neu, P. Maletinsky, and R. J. Warburton, Deterministic Enhancement of Coherent Photon Generation from a Nitrogen-Vacancy Center in Ultrapure Diamond, Phys. Rev. X **7**, 031040 (2017).
[65] E. Togan, Y. Chu, A. S. Trifonov, L. Jiang, J. Maze, L. Childress, M. G. Dutt, A. S. Sørensen, P. R. Hemmer, A. S. Zibrov, and M. D. Lukin, Quantum entanglement between an optical photon and a solid-state spin qubit, Nature (London) **466**, 730 (2010).
[66] W. Gao, P. Fallahi, E. Togan, J. Miguel-Sánchez, and A. Imamoglu, Observation of entanglement between a quantum dot spin and a single photon, Nature (London) **491**, 426 (2012).
[67] P. C. Humphreys, N. Kalb, J. P. Morits, R. N. Schouten, R. F. Vermeulen, D. J. Twitchen, M. Markham, and R. Hanson, Deterministic delivery of remote entanglement on a quantum network, Nature (London) **558**, 268 (2018).
[68] R. Stockill, M. J. Stanley, L. Huthmacher, E. Clarke, M. J. Hugues, A. Miller, C. Matthiesen, C. Le Gall, and M. Atatüre,

Phase-Tuned Entangled State Generation between Distant Spin Qubits, Phys. Rev. Lett. **119**, 010503 (2017).

[69] D. Buterakos, E. Barnes, and S. E. Economou, Deterministic Generation of All-Photonic Quantum Repeaters from Solid-State Emitters, Phys. Rev. X **7**, 041023 (2017).

[70] C. P. Michaels, J. A. Martínez, R. Debroux, R. A. Parker, A. M. Stramma, L. I. Huber, C. M. Purser, M. Atatüre, and D. A. Gangloff, Multidimensional cluster states using a single spin-photon interface coupled strongly to an intrinsic nuclear register, Quantum **5**, 565 (2021).